Comprehensive Analysis of Single-Particle Growth in Heterogeneous Olefin Polymerization: The Random-Pore Polymeric Flow Model

Vassileios Kanellopoulos,[†,‡] Georgios Dompazis,[†,‡] Bill Gustafsson,[§] and Costas Kiparissides*[,†,‡]

Department of Chemical Engineering, Aristotle University of Thessaloniki, and Chemical Process Engineering Research Institute, P.O. Box 472, Thessaloniki, Greece 540 06, Borealis Corporate Research and Development, P.O. Box 330, Porvoo FIN-06101, Finland

In the present study, a comprehensive mathematical model is developed to analyze the effects of initial catalyst size, active site concentration, catalyst morphology (e.g., porosity, extent of prepolymerization, etc.), and hydrodynamic conditions on the growth and overheating of highly active Ziegler−Natta catalyst particles (e.g., fresh or prepolymerized) in gas-phase olefin polymerization. The generalized Stefan−Maxwell diffusion equation for porous solids is combined with the mass balances on the various molecular species (i.e., monomer and "live" and "dead" polymer chains) and the energy conservation equation to predict the temporal−spatial evolution of temperature and monomer concentration, as well as the polymerization rate in a single catalyst/polymer particle. To calculate the equilibrium monomer concentration in the amorphous polymer phase, the Sanchez−Lacombe equation of state is employed. It is shown that the evolution of the catalyst/particle morphology greatly affects the internal and external mass- and heat-transfer resistances in the particle and, thus, its growth rate and overheating. The effect of the hydrodynamic flow conditions on particle overheating is analyzed in detail. It is shown that, depending on the particle size, the concentration of solids in the bulk gas phase, and the dissipation rate of the turbulence kinetic energy of the flow field, the Ranz−Marshall correlation can significantly underestimate the value of the heat-transfer coefficient, resulting in an erroneous overestimation of the particle temperature.

Introduction

In the past 15 years, significant advancements have been made in the manufacturing of polyolefins by low-pressure catalytic processes. The evolution of traditional Ziegler−Natta catalysts as well as the introduction of metallocene-based catalytic systems along with new process improvements (e.g., condensed-mode operation) have made possible the production of polyolefins with desired molecular architectures [e.g., molecular weight distribution (MWD), copolymer composition distribution (CCD), stereoregularity, etc.] at very high rates. Typical heterogeneous Ziegler−Natta catalysts, used in gas-phase olefin polymerization reactors, consist of $TiCl_3$ and TEA ($AlEt_3$) supported on porous $MgCl_2$ or silica particles in the size range of 30−100 μm. Polymerization proceeds at the active catalyst Ti sites distributed throughout the external and internal surface area of the porous support. The polymer formed inside the catalyst pores at the very early stages of the polymerization results in catalyst fragmentation and the formation of a large number of microparticles. As the reaction proceeds, the catalyst microparticles are encapsulated by the growing polymer chains, leading to the formation of a pseudohomogeneous polymer macroparticle and the decrease of particle porosity.

A great number of publications have appeared in the open literature dealing with the mathematical modeling of the growth of a single polymer particle in heterogeneous Ziegler−Natta olefin polymerizations.[1−5] Among the various single-particle growth models, the multigrain model (MGM)[2,6] and the polymeric flow model (PFM)[1,7] are considered to be the closest approximations of the actual physical and chemical phenomena taking place in a growing polymer particle. Both models can provide estimates of the overall particle polymerization rate and spatial distribution of temperature and monomer and polymer molecular properties via the solution of a system of partial differential equations describing the conservation of energy and various molecular species in the growing polymer particle. The MGM incorporates a more detailed picture of the diffusion phenomena occurring at both the micro- and macroparticle levels that considerably increases its mathematical complexity and the computational effort. On the other hand, the PFM offers the advantage of a relatively simpler mathematical formulation via the hypothesis of the pseudohomogeneous reaction medium that greatly facilitates the numerical solution of the resulting moving boundary value problem.

It should be pointed out that, at very high polymerization rates [e.g., over 30000 g/(g_{cat}·h)], internal and external mass- and heat-transfer phenomena become extremely important, and thus, they need to be carefully taken into account. In a recent publication by McKenna et al.,[8] it was shown that, for highly active catalysts, model predictions obtained from the solution of the MGM and PFM significantly deviated from experimen-

* To whom correspondence should be addressed. Tel.: + 30 2310 996211. Fax: +30 2310 996198. E-mail: cypress@alexandros.cperi.certh.gr.
† Aristotle University of Thessaloniki.
‡ Chemical Process Engineering Research Institute.
§ Borealis Corporate Research and Development.

10.1021/ie030810u CCC: $27.50
Published on Web 07/21/2004

tal observations on the polymerization rate for both gas-phase and slurry catalytic olefin polymerization. Furthermore, they postulated that the use of the Ranz−Marshall correlation for calculating the external film heat-transfer coefficient resulted in unrealistically high predictions of the particle temperature. In addition to the above modeling uncertainties regarding the calculation of the solid−gas heat-transfer coefficient, the calculation of the actual monomer concentration at the catalyst active sites and the accurate prediction of the effective monomer diffusion coefficient during the growth of a polymer particle are two issues that need to be properly addressed in any particle growth modeling study. In a more recent publication by Parasu Veera at al.,[9] the MGM was appropriately revised so that it could account for monomer transport by convection through the interstitial pores of the particle. It was shown that monomer convection through the particle's pores substantially contributed to the total monomer transport to the active sites. However, this work did not consider any change in the effective monomer diffusion coefficient during polymerization due to the evolution of the particle morphology. Kosek et al.[10] used two different models, namely, the dusty gas model and a Fickian diffusion model, to show that the convective flow of species in the particle pores, driven by a pressure gradient caused by the change in the reaction stoichiometry (i.e., in the number of moles), resulted in a substantial increase of the particle temperature.

It is important to point out that one of the major drawbacks of the above modeling studies is the lack of a fundamental transport model accounting for the multicomponent diffusion of reactive and inert species in the pores and the amorphous phase of a growing semicrystalline polymer particle. Moreover, the calculation of the solid−gas external heat-transfer coefficient in terms of the actual hydrodynamic flow conditions is an issue that must be properly addressed in any single-particle growth modeling study. Unfortunately, in most theoretical studies on single-particle growth, the Ranz−Marshall correlation has been exclusively employed, resulting in a significant underestimation of the heat-transfer coefficient.

In the present study, a comprehensive single-particle growth model is developed to investigate the effects of the initial catalyst size, active site concentration, catalyst/particle morphology, degree of polymer crystallinity, monomer sorption kinetics, catalyst prepolymerization conditions, and hydrodynamic flow conditions on the growth and overheating of highly active Ziegler−Natta catalysts in gas-phase olefin polymerizations. To describe ethylene polymerization over a heterogeneous Ziegler−Natta catalyst, a simplified polymerization kinetic scheme is considered. The generalized Stefan−Maxwell diffusion equation is combined with the dynamic energy and mass balance equations on the various molecular species to predict the spatial−temporal evolution of the temperature, the concentrations of the various species, and the overall polymerization rate in a single catalyst/polymer particle. To calculate the monomer concentration in the amorphous polymer phase, the Sanchez−Lacombe equation of state (EOS) is employed.[11,12] Because the effective monomer diffusion coefficient exhibits a significant variation during the growth of a catalyst particle, a detailed analysis is carried out to assess the effects of particle morphology on the polymerization rate and temperature in a single particle. Furthermore, to account for the effect of monomer sorption kinetics on the initial catalyst/particle growth rate, a Langmuir-type sorption isotherm equation is imposed on the nonisothermal random-pore polymeric flow model (RPPFM) as an external boundary condition. Finally, a new correlation is proposed for the calculation of the external gas−solid heat-transfer coefficient.[13] In the new correlation, the Reynolds number is expressed in terms of the energy dissipation rate of the turbulence kinetic energy. As a result, the effect of the solids concentration on the external film heat-transfer coefficient can be taken into account via the change in the energy dissipation rate of the continuous phase.

The paper is organized into four sections. In the following section, the development of the random-pore polymeric flow model (RPPFM) is described. To simplify the numerical solution of the resulting moving boundary value problem, the time-dependent radial integration domain is transformed into a time-invariant domain via the introduction of a new dimensionless radial variable. In the third section, the Sanchez−Lacombe equation of state is employed to calculate the thermodynamic equilibrium concentration of monomer in the amorphous phase of a semicrystalline polymer particle. A new diffusion model is proposed to calculate the effective monomer diffusion coefficient in a porous polymer particle, taking into account the change in particle porosity (e.g., its decrease with polymerization time), the degree of polymer crystallinity, the size of the penentrant molecules, and the temperature. Accordingly, a new correlation is proposed for calculating the gas−solid external heat-transfer coefficient. The effects of the energy dissipation rate and solids concentration in the continuous gas phase on the particle overheating are analyzed in detail. In the final section of the paper, a detailed discussion of the results obtained through the numerical solution of the new comprehensive model is presented.

Single-Particle Modeling

To predict the spatial−temporal evolution of monomer concentration, temperature, and polymerization rate in a single catalyst/polymer particle in gas-phase olefin polymerization, a new model [i.e., the so-called random-pore polymeric flow model (RPPFM)] is proposed. The development of the RPPFM is based on the modified polymeric flow model (MPFM)[1,7] and the random-pore diffusion model of Wacao and Smith.[14] A schematic representation of the RPPFM is presented in Figure 1. The growing polymer particle is assumed to be spherical, and the polymer/catalyst phase is treated as a pseudohomogeneous medium of constant density. In fact, the catalyst/polymer phase is approximated by a series of polymer shells, each one exhibiting evenly distributed properties.[7] Monomer diffusion and heat conduction are assumed to occur only in the radial direction, and diffusion of all the other species (e.g., polymer chains) is considered to be negligible. In the new model (RPPFM), the transfer of the various reactive and inert species from the continuous gaseous bulk phase to the catalyst active sites is assumed to occur via a dual diffusion mechanism (i.e., diffusion through the open catalyst/particle pores and diffusion through the amorphous phase of the semicrystalline polymer). As a result, the overall monomer transport rate will largely depend on the catalyst/particle morphology,

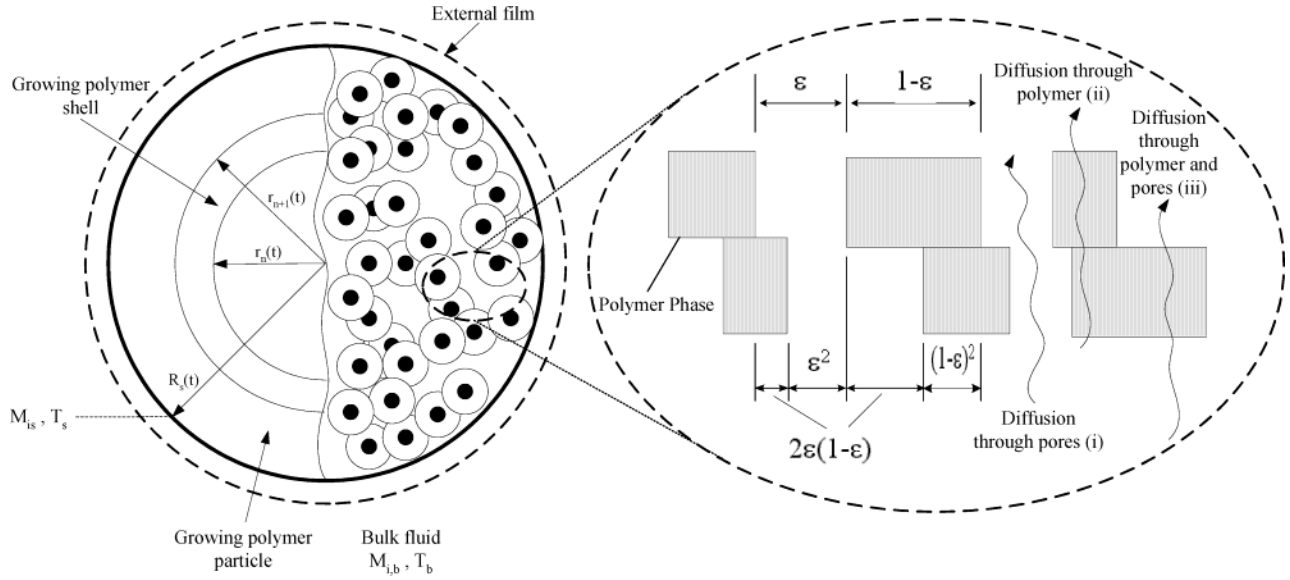

Figure 1. Schematic representation of the random-pore polymeric flow model.

Table 1. Simplified Kinetic Mechanism of Ethylene Polymerization over Ziegler−Natta Catalysts

description	reaction
spontaneous activation	$S_p^k \xrightarrow{k_a^k} P_0^k$
initiation	$P_0^k + M \xrightarrow{k_0^k} P_1^k$
propagation	$P_n^k + M \xrightarrow{k_p^k} P_{n+1}^k$
spontaneous deactivation	$P_*^k \xrightarrow{k_d^k} S_d + D_n$

which continuously changes with polymerization time. Thus, to calculate the overall polymerization rate and the particle temperature, one should faithfully account for the evolution of particle morphology and its effect on the mass- and heat-transfer phenomena occurring in the growing particle.

In what follows, a simplified kinetic mechanism for ethylene polymerization over a heterogeneous Ziegler−Natta catalyst is described. Subsequently, the generalized Stefan−Maxwell diffusion equation is employed to calculate the molar diffusion fluxes of the various molecular species in the pores of the solid particle. Finally, dynamic molar species balances along with an energy conservation equation are derived to describe the space-time evolution of the various reactive species (e.g., monomer, catalyst active sites, etc.) and temperature in a growing catalyst/polymer particle.

Polymerization Rate Functions. In the present study, a simplified two-site kinetic model describing ethylene polymerization over a heterogeneous Ziegler−Natta catalyst is employed. The kinetic mechanism comprises a series of elementary reactions including site activation, propagation, and site deactivation (see Table 1). On the basis of the proposed kinetic mechanism, the net formation rate of "live" polymer chains of length n, at the k type of active sites, can be derived as[15]

$$R_{P_n}^k = -k_d^k P_n^k + \delta(n) k_0^k P_0^k[M] + [1 - \delta(n)] k_p^k P_{n-1}^k[M] - k_p^k P_n^k[M] \quad (1)$$

where $\delta(n)$ is the Kronecker delta function [i.e., $\delta(n) = 1$ for $n = 1$ and $\delta(n) = 0$ for $n \neq 1$]. P_n^k denotes the concentration of live polymer chains of total length n formed at the k type of active site. Similarly, the respective reaction rates for potential, $R_{S_p}^k$, and vacant, $R_{P_0}^k$, active sites, are given by eqs 2 and 3

$$R_{S_p}^k = -k_a^k S_p^k \quad (2)$$

$$R_{P_0}^k = k_a^k S_p^k - (k_0^k[M] + k_d^k) P_0^k \quad (3)$$

Accordingly, the net ethylene consumption rate, R_{Mi} [mol/(m_{polym}^3·s)], can be expressed as

$$R_{Mi} = \sum_{k=1}^{N_s} [M](k_0^k P_0^k + k_p^k \lambda_0^k) \quad (4)$$

where N_s is the number of catalyst active sites; P_0^k is the concentration of type-k vacant active sites; and λ_0^k denotes the zeroth moment of the total number chain length distribution (TNCLD) of live polymer chains formed at the type-k active sites, defined as

$$\lambda_0^k = \sum_{n=1}^{\infty} P_{n,i}^k \quad (5)$$

Following the development of Hatzantonis et al.,[15] the rate function for the zeroth-order moment of the TNCLD of live polymer chains, at the type-k active sites, can be written as

$$R_{\lambda_0}^k = k_0^k[M] P_0^k - \lambda_0^k k_d^k \quad (6)$$

Random-Pore Polymeric Flow Model. The generalized Stefan−Maxwell diffusion equation provides a consistent framework for calculating the bulk and Knudsen diffusion fluxes of a gaseous mixture in a porous solid particle. Thus, under isobaric conditions, the molar flux of component i is given by the equation[16,17]

$$-C_t \frac{dx_i}{dr} = \sum_{j=1, i\neq j}^{n} \frac{1}{D_{ij}}(x_j N_i - x_i N_j) + \frac{N_i}{D_i^K} \qquad i = 1, 2, ..., n \quad (7)$$

where C_t is the total molar concentration of the penentrants, x_i is the mole fraction of component i, N_i is the molar diffusion flux of component i, and r is the length coordinate in the transport direction. D_{ij} and D_i^K denote the effective binary diffusion coefficient of component i with respect to species j and the Knudsen diffusion coefficient, respectively. An estimate of the Knudsen diffusion coefficient can be obtained with the following equation[18]

$$D_i^K = \frac{d_{pore}}{3}\left(\frac{8RT}{3MW_i}\right)^{0.5} \tag{8}$$

where d_{pore} is an average pore diameter and MW_i is the molecular weight of species i. The estimation of the binary diffusion coefficient D_{ij} in a semicrystalline porous polymer particle is discussed in detail in the following section of this paper.

According to the generalized Graham's law for a gas mixture of n components diffusing through porous solids, the sum of all of the product terms, given by the molar species diffusion flux times the square root of the respective molecular weight, is equal to zero, i.e.

$$\sum_{i=1}^{n} N_i(MW_i)^{1/2} = 0 \tag{9}$$

From eqs 7 and 9, one can easily obtain the following expression for N_i

$$N_i = -\frac{C_t \dfrac{dx_i}{dr}}{\dfrac{1 - g_i x_i}{D_{ij}} + \dfrac{1}{D_i^K}} \tag{10}$$

where

$$1 - g_i x_i = 1 - [1 - (MW_i/MW_j)^{1/2}]x_i \tag{11}$$

Accordingly, an effective overall diffusion coefficient for species i can be defined as

$$D_{i,eff} = \left(\frac{1 - g_i x_i}{D_{ij}} + \frac{1}{D_i^K}\right)^{-1} \tag{12}$$

Thus, using the above definition for $D_{i,eff}$, the molar diffusion flux for component i is written as

$$N_i = -D_{i,eff}\frac{dC_i}{dr} \tag{13}$$

For the reactive-diffusion system schematically shown in Figure 1, the unsteady-state mass balance conservation equation for molecular species i is written as

$$\frac{\partial C_i}{\partial t} = -\frac{1}{r^2}\frac{\partial(r^2 N_i)}{\partial r} + R_{Mi} \tag{14}$$

where R_{Mi} is the net consumption rate of species i. Substituting eq 13 into eq 14, one can easily derive the dynamic molar balance equation for monomer i in the catalyst/polymer particle

Monomer mass balance

$$\frac{\partial C_i}{\partial t} = D_{i,eff}\left(\frac{2}{r}\frac{\partial C_i}{\partial r} + \frac{\partial^2 C_i}{\partial r^2}\right) + \frac{\partial D_{i,eff}}{\partial r}\frac{\partial C_i}{\partial r} + R_{Mi} \tag{15}$$

The numerical solution of eq 15 is subject to following initial and boundary conditions

Initial condition

$$C_i(r,0) = C_{i0} \qquad \text{at } t = 0 \tag{16}$$

Boundary conditions

$$\partial C_i/\partial r = 0 \qquad \text{at } r = 0$$

$$C_i(R_s, t) = C_{is}(1 - e^{-k_s t}) \qquad \text{at } r = R_s(t) \tag{17}$$

where C_{i0} and C_{is} denote the initial monomer concentration in the particle and the thermodynamic equilibrium monomer concentration, respectively. It is important to point out that, because the particle radius, $R_s(t)$, changes with time, the boundary condition for C_i at $r = R_s(t)$ gives rise to a moving boundary value problem. In the present study, it was assumed that the monomer sorption kinetics followed an exponential Langmuir-type isotherm. Thus, the boundary condition for C_i at $r = R_s(t)$ exhibited an exponential dependence on time, reflecting the dynamics of monomer sorption onto the catalyst/particle.

Accordingly, one can easily derive the following partial differential equation to describe the conservation of energy in the growing catalyst/polymer particle

Energy balance

$$\frac{\partial T}{\partial t} = k_e\left(\frac{2}{r}\frac{\partial T}{\partial r} + \frac{\partial^2 T}{\partial r^2}\right) + \frac{1}{\rho_p C_p}\sum_{i=1}^{n} MW_i[(-\Delta H_{r,i})R_{Mi}] \tag{18}$$

where k_e is the thermal conductivity of the polymer [J/(m·s·K)] and $-\Delta H_{r,i}$ is the polymerization heat of monomer i. Similarly, eq 18 is subject to the following initial and boundary conditions

Initial condition

$$T(r,0) = T_0 \qquad \text{at } t = 0 \tag{19}$$

Boundary conditions

$$\partial T/\partial r = 0 \qquad \text{at } r = 0$$

$$-k_e(\partial T/\partial r) = h(T - T_b) \qquad \text{at } r = R_s(t) \tag{20}$$

where h is the external gas−solid-film heat-transfer coefficient [J/(m²·s·K)]. Following the original development of Yiagopoulos et al.,[19] the general dynamic molar balances for potential and vacant active sites and the total concentration of live polymer chains can be written as follows

Mass species balances

$$\frac{\partial C^k}{\partial t} = R_c^k \qquad c = S_p, P_0, \lambda_0 \tag{21}$$

Initial condition

$$C^k(0) = [M_e]_0 A_{sf}^k \qquad \text{at } t = 0 \tag{22}$$

Boundary condition

$$\partial C^k/\partial r = 0 \qquad \text{at } r = 0 \tag{23}$$

S_p^k, P_0^k, and λ_0^k denote the vacant active sites, the live polymer chains, and the catalyst active sites of type k, respectively. R_c^k is the net production rate of the respective molecular species (see eqs 2, 3, and 6). A_{sf}^k is the fraction of total active metal concentration of type k (kmol/kmol of M_e), and $[M_e]_0$ is the initial active metal concentration in the catalyst particle (kmol/m^3), which is assumed to be independent of the radial position.

The overall particle polymerization rate, R_p [kg/(m_{polym}^3·s)] is given by the following integral equation[19]

$$R_p = \frac{\int_{V_p}(\sum_{i=1}^{Nm} MW_i R_{Mi})\, dV}{\int_{V_p} dV} \tag{24}$$

Finally, the local rate of change of the particle radius, r, can be expressed in terms of the local particle polymerization rate, $R_{p,r}$, as

$$\frac{dr}{dt} = \frac{R_{p,r} r}{3\rho_p} \qquad 0 < r \le R_s(t) \tag{25}$$

Thermodynamic and Transport Properties

For the numerical solution of the RPPFM, the thermodynamic and transport properties of the system must be readily available. In particular, to calculate the overall monomer consumption rate in the polymer particle, the concentration of the sorbed monomer at the catalyst active sites should be known (see eq 4). It should be emphasized that the prediction of the effective monomer diffusion coefficient in the catalyst/polymer particle (see eq 12) is a problem that has received little attention despite its importance in the calculation of the monomer transfer rate from the bulk gas phase to the active sites. The estimation of the thermal conductivity of semicrystalline polymers is a subject that is also addressed in this section. Finally, a new correlation that takes into account the hydrodynamic flow conditions around a polymer particle is proposed for the calculation of the gas−solid-film heat-transfer coefficient.

Calculation of the Equilibrium Sorbed Monomer Concentration. In the heterogeneous catalytic polymerization of ethylene, the initially formed polymer is amorphous.[2] However, as the "dead" polymer chains move away from the catalyst active sites as a result of the formation of new polymer, crystallization of the amorphous polyethylene (PE) takes place. Thus, it can be assumed that a growing polymer particle will consist of two phases, namely, a monomer-swollen amorphous PE phase and a crystalline PE phase that acts as a barrier to monomer transport.

In general, Henry's law is be applicable to polymer−vapor systems involving heavier penentrants, high pressures, or/and low temperatures.[20] Furthermore, in the presence of a comonomer (e.g., 1-butene) significant deviations from Henry's law behavior can be obtained in the predicted ethylene solubility values.[19] In the present study, the Sanchez−Lacombe lattice-fluid model was employed to calculate the equilibrium concentration of sorbed ethylene in the amorphous PE phase.[11,12,21] (See Table 2 for the values of parameters for low-density polyethylene (LDPE) and ethylene used in the Sanchez−Lacombe EOS.)

Table 2. Values of LDPE and Ethylene Parameters Used in Sanchez−Lacombe EOS

species	P^* (bar)	T^* (K)	ρ^* (g/cm^3)
LDPE[11]	3595	536	0.959
ethylene[12]	3396	294	0.682

In semicrystalline polymers, sorption occurs only in the amorphous polymer phase.[22] Thus, the ethylene solubility coefficient, S, defined as the mass fraction of sorbed monomer over the total polymer mass, is given by

$$S = a_\varphi S^* \tag{26}$$

where S^* is the ethylene solubility coefficient in the amorphous polymer phase (i.e., the mass fraction of the sorbed monomer over the amorphous polymer mass) and α_φ is the amorphous mass fraction of PE in the semicrystalline polymer particle,[2,23] defined as

$$a_\varphi = \left(\frac{\rho_{crys} - \rho_p}{\rho_{crys} - \rho_{am}}\right)\frac{\rho_{crys}}{\rho_p} \tag{27}$$

ρ_{crys}, ρ_{am}, and ρ_p denote the densities of the crystalline, amorphous, and semicrystalline polymer, respectively. For polyethylene, the corresponding values for ρ_{crys} and ρ_{am} are 0.997 and 0.854 g/cm^3, respectively.[19]

Calculation of the Effective Monomer Diffusion Coefficient. One of the most important transport properties for calculating the growth rate of a catalyst/polymer particle in gas-phase olefin polymerization is the effective monomer diffusion coefficient. In general, the monomer diffusivity is a complex function of the particle morphology (e.g., particle porosity), the molecular and physical properties of PE (e.g., molecular weight of PE, degree of crystallinity), and the temperature. Notice that the monomer diffusion coefficient will vary with time and radial position during the growth of a polymer particle.

In general, there is great uncertainty regarding the variation of the effective monomer diffusivity in catalyzed olefin polymerizations. Floyd et al.[24] reported that the effective ethylene diffusivity in PE can vary from 10^{-5} to 10^{-7} cm^2/s. More recently, Kiparissides et al.[25] measured the ethylene diffusion coefficient in semicrystalline polyethylene films at elevated temperatures and pressures, using a magnetic suspension microbalance. They reported that the effective ethylene diffusivity in the amorphous PE could vary from 1×10^{-7} to 1×10^{-6} cm^2/s.

Han-Adebekun[26] studied the effect of polymerization temperature on PE particle morphology and monomer diffusivity using a novel experimental temperature-perturbation technique. To explain her experimental observations on the effective monomer diffusivity, she[26] employed a steady-state isothermal multigrain model assuming a single monomer diffusion coefficient. It was found that, at low polymerization temperatures, the measured effective ethylene diffusivity remained constant and had a value of about 10^{-3} cm^2/s, a value close to the ethylene bulk diffusivity.[25] However, at high polymerization temperatures (i.e., $T > 90$ °C), the effective ethylene diffusivity exhibited a sharp decrease while its value was close to that in the amorphous PE (i.e., $\sim 10^{-7}$ cm^2/s). Furthermore, it was found that the

internal pore volume of the polymer particles decreased as the polymerization temperature increased, resulting in a dramatic decrease of the monomer diffusivity due to pore "filling". It is important to point out that, despite the importance of the monomer diffusion coefficient in calculations of the growth rate and particle overheating of highly active catalysts, the problem has not been incorporated into previous modeling studies in a comprehensive way. In fact, the effect of particle morphology (e.g., porosity, crystallinity) on the catalyst/particle growth rate has often been overlooked, leading to erroneous predictions of particle growth rate and particle overheating. Moreover, the presence of other penentrants (e.g., nitrogen) in addition to monomer(s) has not been taken into account in the calculation of the effective monomer diffusion coefficient.

As pointed out in the previous section, monomer transfer from the bulk gas phase to the active catalyst sites is assumed to occur via a dual-transport mechanism: (i) monomer diffusion through the open pores (i.e., macro- and micropores) of the growing particle and (ii) monomer diffusion through the amorphous regions of the semicrystalline polymer particle. As mentioned in the Introduction, at the very early stages of the polymerization, the catalyst undergoes controllable fragmentation resulting in a large number of microparticles that are subsequently encapsulated by the polymer chains.[2] During this early particle growth period, the available pore volume can be as large as 0.14 cm^3/g. Thus, monomer transfer primarily occurs through the particle's open pores. However, as the polymerization proceeds (i.e., the volume of the polymer phase increases), the mode of monomer transport shifts from diffusion through the open pores to diffusion through the amorphous polymer phase.

According to the general gas diffusion theory of Chapman and Enskog, the binary diffusion coefficient of species i in the presence of another penetrant j is given by the following equation[18,27,28]

$$D_{ij}^0 = 1.86 \times 10^{-3} T^{3/2} \left(\frac{1}{\mathrm{MW}_i} + \frac{1}{\mathrm{MW}_j} \right)^{1/2} / P \sigma_{ij}^{\ 2} \Omega \quad (28)$$

where P, MW_i, and MW_j are the pressure and the molecular weights of the penentrants, respectively. The dimensionless quantity Ω is a complex function of the Leonard-Jones 12−6 potential, temperature, and energy of interaction between the two species (i, j). The mean collision diameter, σ_{ij}, is equal to the arithmetic average of the respective collision diameters of the two penentrants

$$\sigma_{ij} = (\sigma_i + \sigma_j)/2 \quad (29)$$

As the polymer phase grows or/and the particle temperature increases, the continuously formed amorphous polymer fills the pores of the particle. As a result, monomer mass transfer will also take place through the amorphous phase of the polymer. In the latter case, the ethylene diffusion coefficient in the polymer phase will depend on the temperature, the concentration of sorbed ethylene, and the degree of crystallinity. According to Doong and Ho,[29] the diffusion coefficient, D_i^{p}, of small penetrant molecules i in the amorphous polymer phase can be expressed as the product of two terms

$$D_i^{\mathrm{p}} = D_{\mathrm{d}}(d,T,\varphi_{\mathrm{c}})\, f(\varphi_1,\varphi_{\mathrm{c}}) \quad (30)$$

where $D_{\mathrm{d}}(d,T,\varphi_{\mathrm{c}})$ is the thermodynamic diffusion coefficient at zero penetrant concentration and $f(\varphi_1,\varphi_{\mathrm{c}})$ is a correction factor that accounts for the plasticizing effect of the sorbed penetrant. d, φ_1, φ_{c}, and T denote the diameter of the spherical penetrant molecules, the concentration of the penetrant expressed as the volume fraction of the penetrant in the amorphous polymer phase, the volume fraction of the crystalline phase, and the temperature, respectively.[25]

To take into account the dual mode of monomer transport from the bulk gas phase to the catalyst active sites (i.e., via the particle's pores and the amorphous polymer phase), the random-pore model of Wacao and Smith was employed.[16,30] A schematic representation of the random-pore model of Wacao and Smith is presented in Figure 1. As can be seen, three diffusion paths through the two hypothetical consecutive layers of microparticles can be identified: (i) diffusion through the open pores, (ii) diffusion through the amorphous polymer domains, and (iii) diffusion through the pores of one layer and the amorphous polymer phase of the next.

It is apparent that the selected arrangement of the pores in the RPPFR (see Figure 1) does not represent the real pore geometry in the growing particle. Furthermore, the pores are not parallel to the direction of diffusion. Thus, a tortuosity factor, τ_{f}, is introduced to take into account the tortuous nature of the pores and the presence of random constrictions in the pore geometry. Because the diffusion rate through the pores is higher than that through the polymer phase, one can show that the overall monomer binary diffusivity, D_{ij}, in the particle can be expressed as follows[14]

$$D_{ij} = \frac{\epsilon}{\tau_{\mathrm{f}}^{\ 2}} D_{ij}^0 + (1-\epsilon)(1+3\epsilon) D_i^{\mathrm{p}} \quad (31)$$

Notice that the first term on the right-hand side of eq 31 accounts for the monomer mass transfer via the particle's void fraction while the second term accounts for the monomer transport through the amorphous polymer phase. Thus, the overall effective diffusivity of ethylene in PE, $D_{i,\mathrm{eff}}$, can be calculated by substituting eq 31 into eq 12. It should be pointed out that, during the particle's growth lifetime, the effective ethylene diffusivity, $D_{i,\mathrm{eff}}$ will vary from its initial value in the fresh catalyst, $(\epsilon/\tau_{\mathrm{f}}^{\ 2})D_{ij}^0$, to its limiting thermodynamic value in the polymer phase, D_i^{p}.

Calculation of the Polymer Thermal Conductivity. Although no fundamental theory exists for the accurate prediction of the thermal conductivity in semicrystalline polymers, several investigators have employed the following expression for the calculation of the thermal conductivity of amorphous polymers based on Debye's treatment of heat conductivity[31,32]

$$k_{\mathrm{am}} = C_{\mathrm{p}} \rho_{\mathrm{am}} L (U_{\mathrm{R}}/V_{\mathrm{am}})^3 \left[\frac{3(1-\nu_{\mathrm{s}})}{1+\nu_{\mathrm{s}}} \right]^{1/2} \quad (32)$$

where k_{am}, V_{am}, and U_{R} are the thermal conductivity in J/(s·m·K), the molar volume of the amorphous polymer, and the molar velocity of sound, respectively. According to Krevelen,[32] for solid polymers, the term $[3(1-\nu_{\mathrm{s}})/(1+\nu_{\mathrm{s}})]^{1/2}$ is approximately equal to 1.05, and the value of L is about 5×10^{-11} m. On the other hand, the value of U_{R} can be calculated via the group contribution

method.[32] For polyethylene, the value of U_R is equal to 1760 $(cm^3/mol)(cm/s)^{1/3}$.[32]

For crystalline polymers, the following expression has been proposed for the calculation of the thermal conductivity[31]

$$\frac{k_{crys}}{k_{am}} = 1 + 5.8\left(\frac{\rho_{crys}}{\rho_{am}} - 1\right) \tag{33}$$

where k_{crys} is the thermal conductivity of the crystalline polymer in J/(s·m·K). For semicrystalline polyethylene, Krevelen[32] proposed the following expression for the calculation of the thermal conductivity of the polymer, k_e

$$\frac{k_e}{k_{am}} = \frac{2k_{am} + k_{crys} + 2\varphi_{crys}(k_{crys} - k_{am})}{2k_{am} + k_{crys} - \varphi_{crys}(k_{crys} - k_{am})} \tag{34}$$

φ_{crys} is the crystalline volume fraction. Notice that, as the temperature increases, k_{crys} increases, whereas k_{am} decreases slightly. Thus, k_e can either increase or decrease with increasing temperature, depending on the degree of crystallinity of the polymer.[31,32]

External Heat- and Mass-Transfer Coefficients. In the past 50 years, various correlations have been proposed in the open literature for the calculation of the gas−solid-film mass- and heat-transfer coefficients for spherical particles in a flowing gas medium. However, depending on the selected mass- and heat-transfer correlations, the calculated values of the gas−solid-film heat- and mass-transfer coefficients for small-size particles (i.e., <20 μm) and low Reynolds numbers can differ from the actual ones by several orders of magnitude.[33]

In gas-phase catalytic olefin polymerization, several investigators[2,4−6,24] have employed the Ranz−Marshall correlations to calculate the gas−solid-film mass- and heat-transfer coefficients for growing polymer particles. Although the mass-transfer resistance in the film surrounding a growing polymer particle can be considered to be negligible, the external film heat-transfer resistance can be significant, especially for small but highly active catalyst particles. For a single particle placed in a continuous gas phase moving with a relative gas to particle velocity of u_r, the well-known Ranz−Marshall correlations for the dimensionless heat- and mass-transfer coefficients are[34]

$$Nu = 2 + 0.6Pr^{1/3}Re^{0.5}$$

$$Sh = 2 + 0.6Sc^{1/3}Re^{0.5} \tag{35}$$

where $Nu = d_p h/k$, $Sh = k_{ext}d_p/D_f$, $Re = d_p u_r \rho_g/\nu_g$, $Pr = \mu_g C_g/k_g$, and $Sc = \mu_g/\rho_g D_f$ are the respective dimensionless Nusselt, Sherwood, Reynolds, Prandtl, and Scmidt numbers.

In general, the above correlations can also be used with dilute dispersions as long as the relative velocity, u_r, is known. For large particles, it has been found that the Ranz−Marshall correlations often provide good predictions of the gas−solid-film heat- and mass-transfer coefficients. Several other correlations have been proposed for specific applications (e.g., in fluidized- and fixed-bed reactors).[35]

Heat- and mass-transfer correlations that include the energy dissipation rate as the fundamental driving force can work very well for a wide variety of reactors and operating conditions. Recent experimental studies on the calculation of particle to gas heat-transfer coefficient in various reactors (e.g., bubble columns, mixing vessels, and fluidized beds) have revealed that the heat-transfer coefficient for a specific application can be obtained by the same correlation as long as the Reynolds number is expressed in terms of the appropriate energy dissipation rate. In a recent publication by Nicolella et al.,[13] the following correlation was postulated for the calculation of the film heat-transfer coefficient in dispersed gas−solid systems

$$Nu = 2 + 0.265(d_p\epsilon_s/\nu^3)^{0.241}\, Pr^{1/3} \tag{36}$$

It should be noted that, for highly concentrated dispersed systems, the energy dissipation rate, ϵ_s, will depend on the concentration of solid particles. Hetsroni[36] developed the following expression to calculate the change in the energy dissipation rate in terms of the concentration of solid particles in fluidized-bed reactors

$$\frac{\epsilon_{s,d}}{\epsilon_s} = \frac{2C_M}{C_o^{0.5}(1 + C_o^{0.25}\bar{\tau}_p\bar{k}^{0.5}/\bar{l})} \tag{37}$$

where ϵ_s and $\epsilon_{s,d}$ denote the energy dissipation rates of the carrier fluid free of solids and of the dispersed system, respectively. C_o is a constant. The dimensionless quantities $\bar{\tau}_p$, $\bar{k}$, and $\bar{l}$ denote the particle response time, the turbulence modulation, and the macroscale mixing length, respectively.[36]

The influence of solid particles on the turbulence kinetic energy of the continuous phase, known as turbulence modulation, is commonly expressed by the ratio $k_t/k_{t,0}$. Crowe et al.[37] proposed the following correlation for the turbulence modulation ratio, $k_t/k_{t,0}$, in a vertical fluidized-bed reactor

$$\left(\frac{k_t}{k_{t,0}}\right)^{3/2} = \frac{1 + 0.55C_M\left(\frac{2gR_{bed}}{u_r^2}\right)^{1.6}\left(\frac{2\rho_c u_r R_{bed}}{\mu_c}\right)^{0.2}\left(\frac{l}{2R_{bed}}\right)^{1.8}\sigma_0^{-3}\left(\frac{d_p}{l}\right)^{0.8}}{1 + \left(\frac{\rho_c}{\rho_d}\right)^{1/3}C_M^{1/3}\left(\frac{d_p}{l}\right)^{-1.0}} \tag{38}$$

where σ_0, ρ_c, ρ_d, and C_M denote the turbulence intensity of the particle-free flow field, the density of the continuous phase, the density of the dispersed phase, and the mass concentration of the solid particles, respectively.

Results and Discussion

The developed random-pore polymeric flow model (RPPFM) was subsequently employed to analyze the effects of the initial catalyst size, partial pressure of the diluent (i.e., nitrogen), monomer sorption kinetics, evolution of the catalyst/particle morphology (i.e., porosity and polymer crystallinity), and hydrodynamic conditions on the growth and overheating of highly active Ziegler−Natta catalysts in the gas-phase polymerization of ethylene. In Tables 3 and 4 are reported the numerical values of the kinetic rate constants and the physical and transport properties of the catalytic polymerization system. Details regarding the numerical simulation of the RPPFM are given in the Appendix A.

Table 3. Numerical Values of the Kinetic Rate Constants[a,b]

rate constant (L/mol·s)	site 1	site 2
activation, k_a[c]	10^3	10^3
initiation, k_0	10^3	10^3
propagation, k_p	10^3	10^3
deactivation, k_d[c]	7×10^{-5}	7×10^{-5}

[a] $T_{ref} = 315.15$ K [b] All activation energies = 10 kcal/mol. [c] Units of 1/s.

Table 4. Numerical Values of the Physical and Transport Properties of the Reaction Mixture

Transport Properties	
T_b (K)	337.15
$[M]_b$ (mol/L)	0.40
$\Delta H_{r,i}$ (cal/g)	−916
C_g (cal/mol·K)	11
μ_g (g/cm·s)	1.16×10^{-4}
k_g (cal/cm·s·K)	5×10^{-5}
u_r (cm/s)	20
Catalyst Parameters	
d_{cat} (μm)	30
d_{pore} (μm)	0.1
ρ_{cat} (g/cm^3)	2.84
$[M_e]_0$ (mol/cm$_{cat}^3$)	1×10^{-5}
A_{sf}^1	0.5
A_{sf}^2	0.5
Polymer Properties	
ρ_{am} (g/cm^3)	0.854
ρ_{crys} (g/cm^3)	0.98
ρ_p (g/cm^3)	0.96
C_p (cal/g·K)	0.44

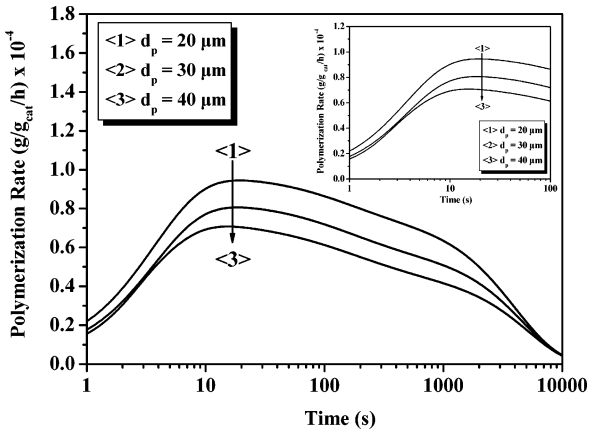

Figure 2. Effect of initial catalyst size on the particle polymerization rate.

Effect of Initial Catalyst Size. The evolution of the polymerization rate and temperature in a single growing polymer particle depend on the initial size of the catalyst and its active metal concentration. In Figure 2, the effect of the initial catalyst size on the polymerization rate−time histories is illustrated. In the simulations, the catalyst active metal concentration remained constant (i.e., $[M_e]_0 = 10^{-5}$ mol/cm$_{cat}^3$). This means that the total molar mass of the active metal increased with the initial size of the catalyst. As can be seen from Figure 2, as the initial catalyst size increases, the polymerization rate initially decreases as a result of mass-transfer limitations. That is, the rate of monomer transfer from the bulk gas phase to the active catalyst sites becomes the limiting step in the polymerization. In Figure 3, the time evolution of the ethylene concentration profiles in the catalyst/polymer particle is plotted as a function of the dimensionless particle radius. It is apparent that,

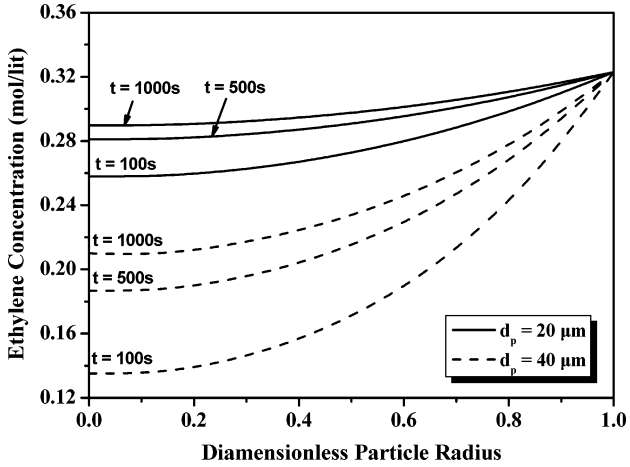

Figure 3. Spatial ethylene concentration profiles for two different catalyst sizes at three different instances.

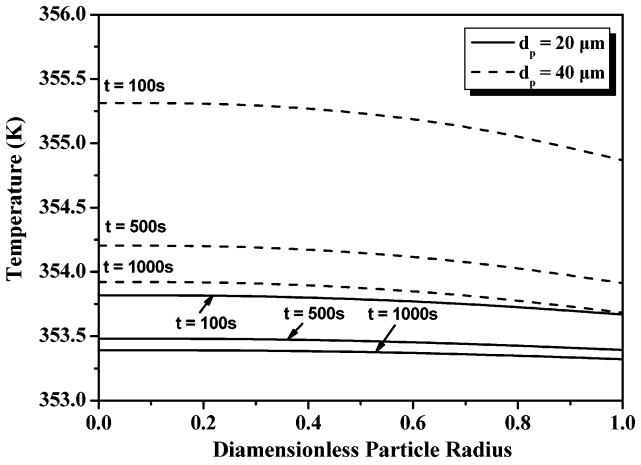

Figure 4. Spatial temperature profiles for two different catalyst sizes at three different instances.

as the initial catalyst size increases, the ethylene concentration in the particle decreases (i.e., because of mass-transfer limitations). As a result, large radial concentration gradients can arise inside the catalyst/polymer particle during the early stages of polymerization. This means that the time required for the elimination of the ethylene concentration radial gradients in the particle increases as the initial catalyst size increases.

On the other hand, no significant radial temperature gradients arise inside the catalyst/polymer particle, even at early polymerization times, according to the results of Figure 4. However, despite the fact that the polymerization rate decreases as the catalyst size increases, particle overheating (i.e., the difference between the particle's surface temperature, T_s, and the temperature in the bulk gas phase, T_b) increases because of heat-transfer limitations (see Figure 5). The results of Figure 5 can be better explained in terms of the particle heat removal rate [i.e., $\dot{Q}_r = hA_p(T_s - T_b)$] and the polymerization heating rate [i.e., $\dot{Q}_g = (-\Delta H_{r,p})V_p r_p$]. In Figure 6, the variation of the ratio $\dot{Q}_g/\dot{Q}_r$ is plotted with respect to the polymerization time for three initial catalyst sizes. It is apparent that as the initial catalyst size increases the value of the $\dot{Q}_g/\dot{Q}_r$ ratio increases, leading to a corresponding increase of particle overheating (see Figure 5). However, as the polymerization continues and the particle's surface area increases, the heat removal rate, $\dot{Q}_r$, asymptotically approaches the polymerization

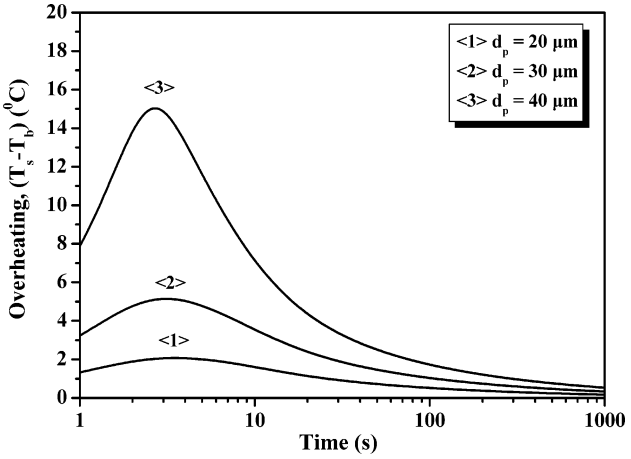

Figure 5. Effect of initial catalyst size on particle overheating.

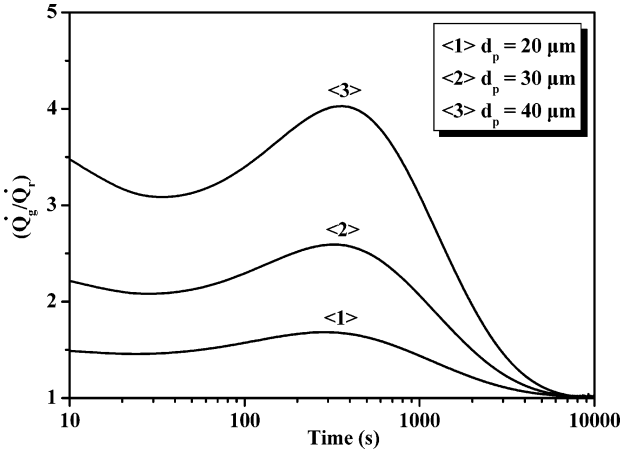

Figure 6. Time evolution of the ratio $\dot{Q}_g/\dot{Q}_r$ for three catalyst sizes.

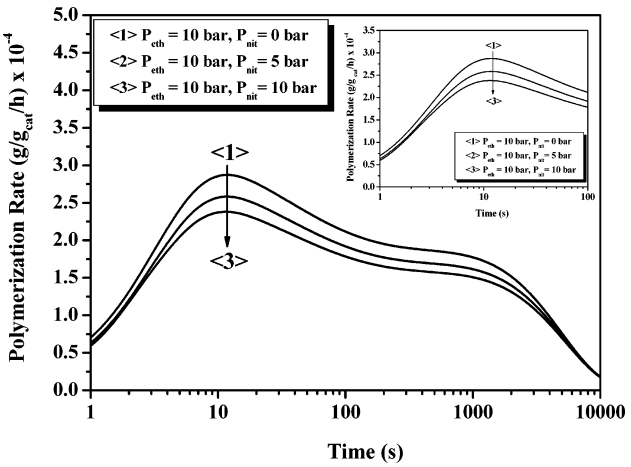

Figure 7. Effect of nitrogen partial pressure on the particle polymerization rate.

heat rate, $\dot{Q}_g$. As a result, the particle temperature approaches that in the bulk gas phase [i.e., $(T_s - T_b) \rightarrow 0$].

Effect of Nitrogen Concentration. The effects of the nitrogen partial pressure on the polymerization rate and particle overheating are illustrated in Figures 7 and 8, respectively. In all simulations, the partial pressure of ethylene in the gas phase remained the same (i.e., $P_{eth} = 10$ bar), and the initial catalyst size and the active metal concentration were equal to 20 μm and 10^{-5} mol/cm_{cat}^3, respectively. It is apparent that, as the nitrogen

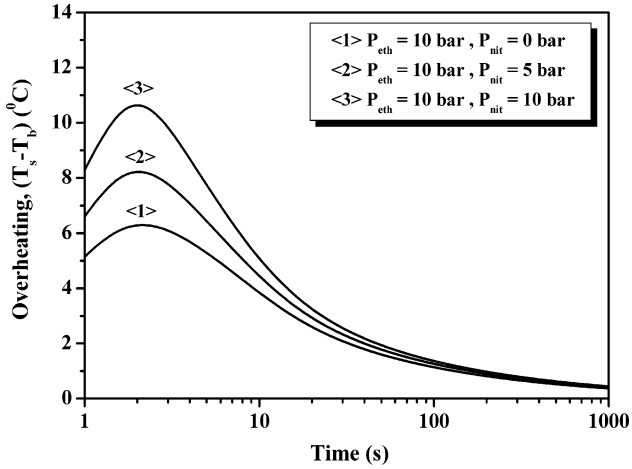

Figure 8. Effect of nitrogen partial pressure on particle overheating.

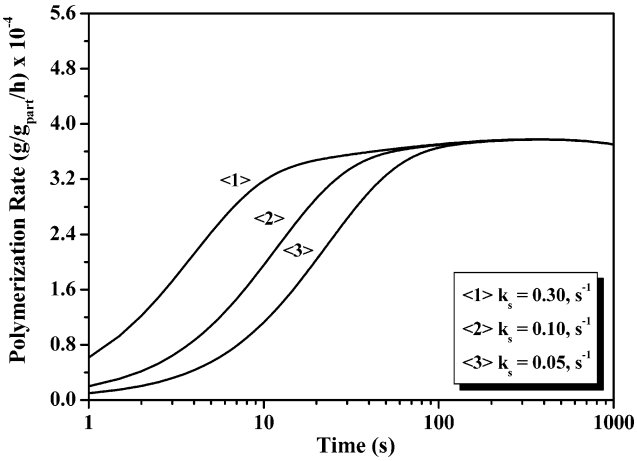

Figure 9. Effect of sorption kinetics on the particle polymerization rate.

partial pressure increases, the polymerization rate decreases as a result of the dilution effect of nitrogen. In fact, the presence of nitrogen inside the catalyst pores introduces an additional resistance to monomer transfer from the bulk gas phase to the active catalyst sites. It should be pointed out that the postulated diffusion model (see eq 12) can explicitly account for the presence of inert species (e.g., nitrogen) in the gas reaction mixture through the use of the generalized Stefan−Maxwell diffusion equation (see eq 10). Notice that particle overheating increases as the nitrogen concentration increases because of the lower rate of increase of the particle's surface area, A_p, which lowers the heat-transfer removal rate, $\dot{Q}_r$.

Effect of Sorption Kinetics. As was mentioned in the Single-Particle Modeling section of the paper, the monomer concentration at the external surface of the particle was assumed to exhibit an exponential Langmuir-type isotherm, reflecting the dynamics of monomer sorption into the catalyst/polymer particle. Thus, the monomer sorption kinetics depended on the sorption rate constant k_s (s^{-1}) (see eq 17). The thermodynamic equilibrium ethylene concentration at the particle's surface, C_{is}, was calculated with the Sanchez−Lacombe EOS.

In Figures 9 and 10, the effects of k_s on the polymerization rate and particle overheating, respectively, are depicted. As can be seen, the monomer sorption kinetics significantly affects the polymerization rate and particle

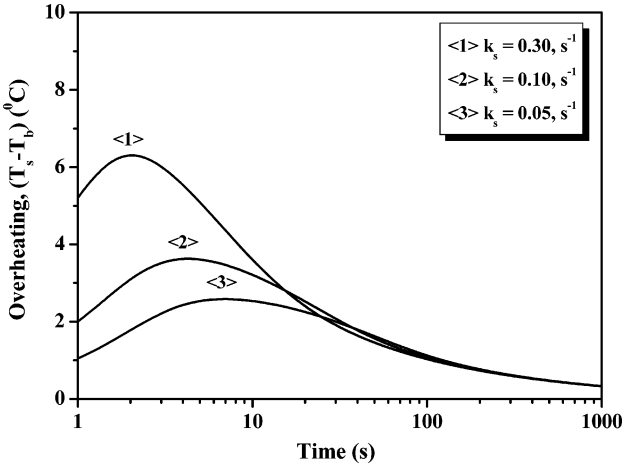

Figure 10. Effect of sorption kinetics on particle overheating.

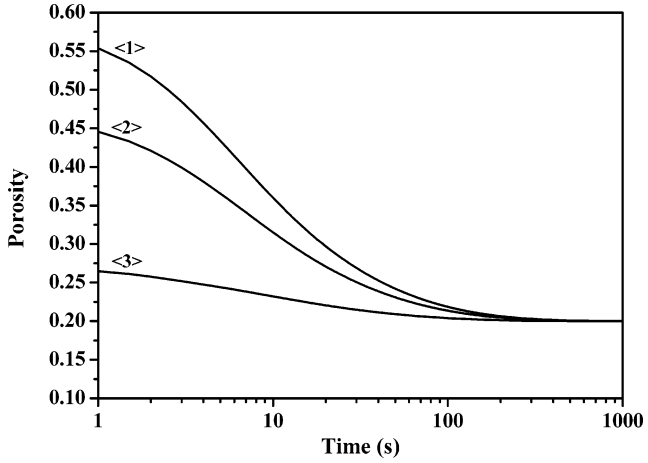

Figure 11. Time evolution of the particle porosity.

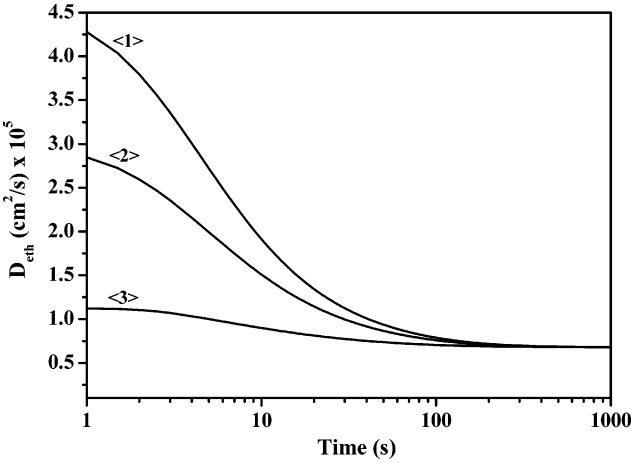

Figure 12. Effect of catalyst/particle morphology on the time evolution of the ethylene diffusion coefficient.

overheating, especially during the first few seconds of the polymerization. Thus, as the value of k_s increases, the monomer concentration at the external particle's surface, C_i, reaches its final thermodynamic value, C_{is}, more quickly. As a result, the time needed for the polymerization rate to attain its maximum value decreases as the value of k_s increases (see Figure 9). On the other hand, the higher the value of k_s is, the larger the particle overheating will be (see Figure 10). From the above results, one can conclude that the catalyst/particle morphology and the sorption kinetics of reactive species [i.e., monomer(s), hydrogen] can significantly affect the polymerization rate and particle overheating in a gas-phase polymerization reactor. In fact, catalyst/polymer particles of the same size fed into a reactor might exhibit different polymerization rates due to differences in the monomer sorption kinetics (i.e., different values of k_s) or/and in the values of the thermodynamic equilibrium monomer concentration, C_{is}. This is further discussed in the subsequent subsection of the paper.

Effect of Particle Morphology/Porosity. The transport of monomer(s) from the bulk gas phase to the catalyst active sites strongly depends on the effective monomer diffusion coefficient. It was earlier shown (see Figure 3) that, at the early stages of polymerization, significant mass-transfer limitations can arise in the growing polymer particle. As pointed out in the previous sections of the paper, the effective monomer diffusion coefficient, $D_{i,\text{eff}}$, depends on the particle's porosity, the degree of polymer crystallinity (i.e., the fraction of the available amorphous polymer phase), the temperature, and the concentrations of the monomer and other inert species (e.g., nitrogen) in the bulk phase. Moreover, the monomer diffusion coefficient will vary with time and radial position during the growth of a catalyst/polymer particle.

According to eqs 12 and 31, the value of the $D_{i,\text{eff}}$ will largely depend on the evolution of the particle's porosity, ϵ. Thus, as the value of ϵ decreases (i.e., as the open pores of the catalyst/particle are filled with polymer), the monomer diffusion coefficient in the particle decreases. This means that rapid and uncontrollable filling of the catalyst's pores during the early stages of polymerization can lead to significant mass-transfer limitations with the concomitant appearance of undesired high particle temperatures (see Figure 5). Therefore, the control of particle morphology (i.e., porosity) during polymerization is of profound importance for both catalyst manufacturers and polyolefin producers.

To further support the above claim, a series of simulations was carried out for different time evolution profiles of the particle's porosity. In Figure 11, the particle porosity is plotted with respect to time for three different pore filling scenarios. In fact, the first scenario represents a relatively slow pore filling case, from an open catalyst/particle structure (i.e., $\epsilon \approx 0.55$) to a closed one (i.e., $\epsilon \approx 0.2$). The second scenario represents an intermediate pore filling process, from a relatively open structure (i.e., $\epsilon \approx 0.45$) to a close one (i.e., $\epsilon \approx 0.2$). Finally, the third scenario represents a very fast pore filling process, in which the particle porosity almost immediately attains its final value. In Figures 12 and 13, the respective time evolutions of the ethylene diffusion coefficient and particle overheating are depicted for the three different pore filling scenarios shown in Figure 11. It is apparent from the results of Figures 11−13 that the faster the pores are filled with polymer, the larger the particle overheating is (because of the faster transition of $D_{i,\text{eff}}$ to its limiting thermodynamic value, D_i^p). In other words, when the catalyst/particle structure is kept open for longer polymerization times, mass-transfer limitations at the particle level and particle overheating are reduced. The above results clearly demonstrate that catalyst design and morphology can have a strong impact on the mass- and heat-transfer phenomena occurring at the early stages of polymerization.

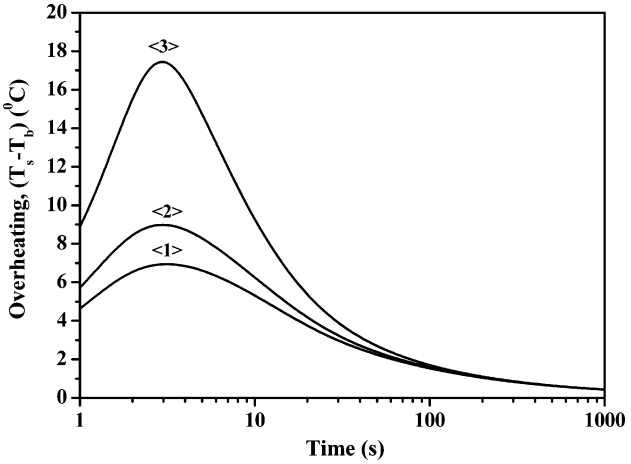

Figure 13. Effect of catalyst/particle morphology on the time evolution of particle overheating.

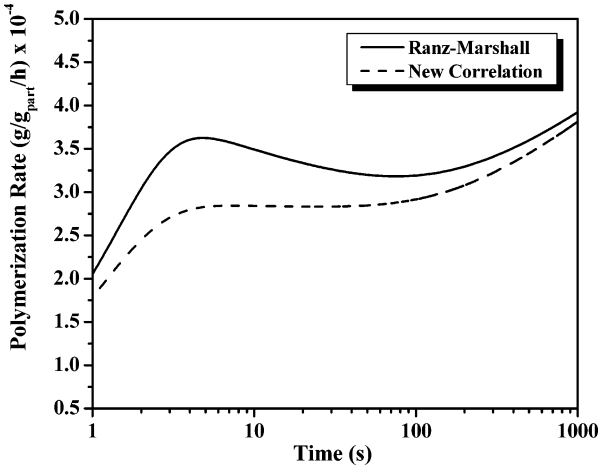

Figure 14. Effect of heat-transfer correlation employed on the time evolution of the particle polymerization rate.

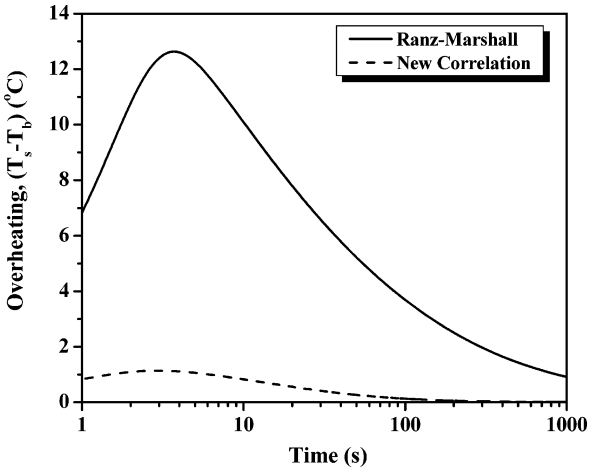

Figure 15. Effect of heat-transfer correlation employed on the time evolution of particle overheating.

Effect of Gas−Solid-Film Heat-Transfer Coefficient. As pointed out in the previous section of this paper, the calculation of the dimensionless heat-transfer coefficient in gas−solid catalytic olefin polymerization systems is a subject that has received little attention despite its importance in the design and operation of fluidized-bed olefin polymerization reactors.

In Figures 14 and 15, the dependences of the polymerization rate and particle overheating, respectively, on the selected heat-transfer correlation are illustrated. In both cases, the size of the prepolymerized catalyst particle was equal to 100 μm. Despite the fact that, at long reaction times (i.e., >1000 s), the calculated values for the polymerization rate for both heat-transfer models (i.e., eqs 35 and 36) are the same, the initially calculated values for particle overheating largely depend on the heat-transfer correlation employed. In fact, the Ranz−Marshall correlation largely underestimates the value of the gas−solid-film heat-transfer coefficient, resulting in a significant overestimation of the particle's temperature (see Figure 15). On the other hand, the Nicolella et al.[13] correlation for the heat-transfer coefficient provides a more realistic estimation of the particle's temperature, as it accounts for the presence of other solids in the gas phase and the resulting enhancement of the heat-transfer coefficient.

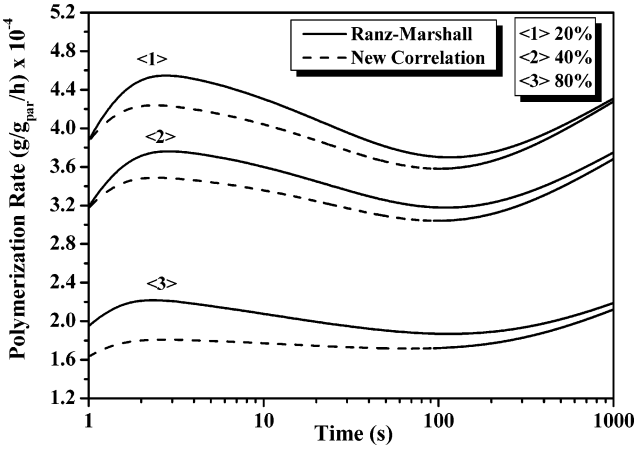

Figure 16. Effect of polymer crystallinity on the time evolution of particle polymerization rate.

Effect of Polymer Crystallinity. It is well-known that the ethylene solubility and permeability in the polymerization system will depend on the extent of polymer crystallinity.[38] In general, the monomer diffusivity will be a complex function of particle morphology (e.g., porosity), degree of crystallinity, partial pressure of ethylene, and temperature. Furthermore, the ethylene solubility in semicrystalline PE depends on the degree of polymer crystallinity, as the presence of a highly crystalline phase limits the swelling of the amorphous polymer phase. To demonstrate the effects of polymer crystallinity on the polymerization rate and particle overheating, several simulation were carried out by varying the degree of crystallinity of a prepolymerized catalyst particle. In all simulations, the size of the prepolymerized particle was equal to 100 μm, and the total active metal content and monomer concentration were 6.2×10^{-10} mol and 0.5 mol/L, respectively. In Figures 16−18, the polymerization rate, the particle overheating, and the effective ethylene diffusivity are plotted with respect to time for three different values of PE crystallinity. The effect of the correlation employed for the calculation of the particle Nusselt number is also depicted in these figures. It should be pointed out that the effective active metal concentration in the amorphous polymer phase (i.e., $[M_e]_{eff} = M_{e,content}/V_{p,am}$) increases as the extent of polymer crystallinity increases, as the active catalyst sites are assumed to be dispersed in only the amorphous polymer phase. As can be seen, the polymerization rate decreases as the extent of crystalline phase in the prepolymerized particle increases despite the fact that the effective active metal

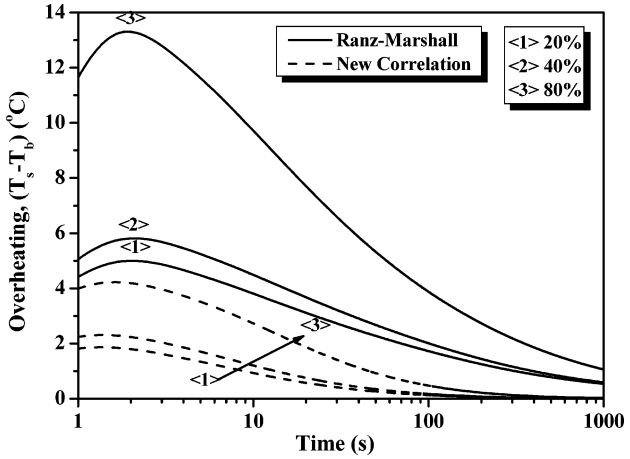

Figure 17. Effect of polymer crystallinity on the time evolution of particle overheating.

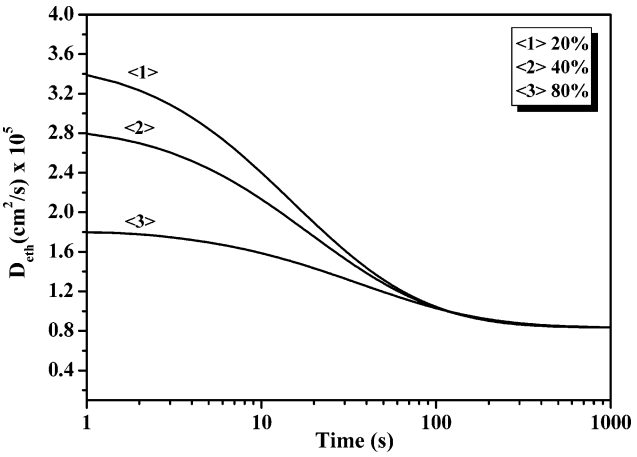

Figure 18. Effect of polymer crystallinity on the time evolution of the ethylene diffusion coefficient.

concentration increases. This can be attributed to the large decrease of the effective ethylene diffusion coefficient (see Figure 18) and the decrease of the effective reaction volume. On the other hand, particle overheating increases as the degree of crystallinity increases because of the lower rate of increase of the particle's surface area, A_p, which lowers the heat removal rate, $\dot{Q}_r$.

It is important to point out that the heat-transfer correlation employed for the calculation of the Nusselt number does not significantly affect the polymerization rate (see Figure 16). On the other hand, it considerably affects the estimation of the particle's temperature (see Figure 17).

Conclusions

A comprehensive single-particle growth model, accounting for both internal and external mass- and heat-transfer resistances, was developed to describe the growth of a single catalyst or/and prepolymerized particle in gas-phase catalyzed olefin polymerization. Extensive simulation studies were conducted to investigate the effects of the initial catalyst size, metal concentration, catalyst/polymer particle morphology, and hydrodynamic conditions on the polymerization rate and particle overheating of highly active Ziegler−Natta catalyst particles (both fresh and prepolymerized). It was shown that both the polymerization rate and particle overheating increase with increasing initial catalyst size and active metal concentration. Furthermore, it was shown that the presence of a diluent (e.g., nitrogen) in the bulk phase introduces an additional resistance to the monomer transfer from the bulk phase to the active metal sites, resulting in an initial decrease of the polymerization rate and an increase of the particle overheating. It was also demonstrated that the monomer sorption kinetics greatly affects the polymerization rate and the particle overheating, especially during the first few seconds of the polymerization, independently of the evolution of the internal particle morphology. Moreover, it was established that, when the catalyst/particle pores are kept open for longer polymerization times, mass-transfer limitations and, thus, particle overheating are reduced. It was shown that the Ranz−Marshall correlation largely underestimates the value of the gas−solid-film heat-transfer coefficient, resulting in a significant overestimation of the particle's temperature. Finally, it was demonstrated that the polymer crystallinity strongly affects the polymerization rate and particle overheating. Thus, it can be concluded that, for highly active Ziegler−Natta catalysts, it is necessary, for both product quality and reactor operability considerations, to control the morphology of the catalyst/polymer particles prior to their injection into the reactor.

Acknowledgment

The authors gratefully acknowledge the European Community for supporting this work under the Growth Project G5RD-CT-2001-00597.

Notation

A_{sf}^k = fraction of metal that can form active sites of type k, kmol/(kmol of M_e)
C_g = heat capacity of the gas, J/(kg·K)
C_i = concentration of penetrant i in the polymer, kmol/m^3
C_{is} = equilibrium concentration of penetrant i in the polymer, kmol/$m_{amorphous\ polymer}^3$
C_M = solids concentration in the fluidized bed, kg/m^3
C_p = heat capacity of the polymer particle, J/(kg·K)
C_t = total molar concentration of the gas mixture, kmol/m^3
D_f = diffusion coefficient in the fluid, m^2/s
D_i^K = Knudsen diffusion coefficient of penetrant i, m^2/s
$D_{i,eff}$ = overall diffusion coefficient of penetrant i within the growing polymer particle, m^2/s
D_{ij}^0 = binary multicomponent diffusion coefficient of pair i, j in the gas, m^2/s
D_{ij} = effective multicomponent diffusion coefficient of pair i, j in the polymer particle, m^2/s
D_i^p = effective diffusion coefficient of penetrant ***i*** in the polymer phase, m^2/s
d_{cat} = initial catalyst diameter, m
d_p = growing polymer particle diameter, m
d_{pore} = average pore diameter, m
g = gravitational acceleration, m/s^2
h = external film heat-transfer coefficient, J/(m^2·s·K)
k_0^k = rate constant of initiation for type-k catalyst active sites, m^3/(mol·s)
k_a^k = rate constant of spontaneous activation for type-k catalyst active sites, 1/s
k_d^k = rate constant spontaneous deactivation for type-k catalyst active sites, 1/s
k_p^k = rate constant of propagation for type-k catalyst active sites, m^3/(mol·s)
k_e = particle thermal conductivity, J/(m·s·K)
k_{ext} = external film mass-transfer coefficient, m/s

k_g = gas thermal conductivity, J/(m·s·K)
k_s = sorption and catalyst activation parameter, 1/s
k_t = turbulence kinetic energy, J
$k_{t,0}$ = turbulence kinetic energy in the particle free flow, J
l = macroscale mixing length, m
$[M_e]$ = active metal concentration, mol/(m_{cat}^3)
$[M_e]_0$ = initial active metal concentration, mol/(m_{cat}^3)
MW_i = molecular weight of penetrant, kg/kmol
N_i = molar diffusion flux of penetrant i, kmol/(m^2·s)
N_s = number of sites
$Nu = hd_p/k_g$ = Nusselt number
P = pressure, Pa
P^* = parameter in the Sanchez−Lacombe model, Pa
P_0^k = concentration of vacant catalyst active sites of type k, kmol/m^3
P_n^k = concentration of live copolymer chains of length n at catalyst active sites of type k, kmol/m^3
$Pr = \mu_g C_g/k_g$ = Prandtl number
R_{bed} = radius of the fluidized-bed reactor, m
r = radial position inside the particle, m
$Re = d_p u_r \rho_g/\mu_g$ = Reynolds number
R_{Mi} = overall consumption rate of monomer, mol/(m^3·s)
R_p = overall polymerization rate, kg/(m^3·s)
R_s = particle radius, m
S = solubility coefficient, mol/($m_{polymer}^3$·Pa)
S^* = solubility coefficient, mol/($m_{amorphous\ polymer}^3$·Pa)
$Sc = \mu_g/\rho_g D_f$ = Scmidt number
$Sh = k_s d_p/D_f$ = Sherwood number
S_p^k = concentration of potential catalyst active sites of type k, kmol/m^3
t = time, s
T = particle temperature, K
T^* = parameter in the Sanchez−Lacombe model, K
T_b = bulk gas-phase temperature, K
U_R = molar sound velocity, $m^{10/3}$/(kmol·$s^{1/3}$)
u_r = relative particle to gas velocity, m/s
x_i = mole fraction of penetrant i
x_j = mole fraction of penetrant j

Greek Symbols

$\Delta H_{r,i}$ = heat of polymerization, J/kg
ϵ = polymer particle porosity
ϵ_s = viscous dissipation rate, m^2/s^3
$\epsilon_{s,d}$ = viscous dissipation rate when particles are present in the fluid, m^2/s^3
λ = live copolymer moment, kmol/m^3
μ = viscosity, kg/(m·s)
ν = kinematic viscosity, m^2/s
ρ = density, kg/m^3
ρ^* = parameter in the Sanchez−Lacombe model, kg/m^3
σ_i = collision diameter of molecule i, m
σ_j = collision diameter of molecule j, m
σ_{ij} = collision diameter of pair i, j, m
τ_f = tortuosity factor
φ_1 = volume fraction of penetrant
φ_c = volume fraction of the polymer phase
φ_{crys} = degree of crystallinity
Ω = collision integral

Subscripts and Superscripts

am = amorphous polymer property
b = bulk phase property
c = continuous phase
cat = catalyst property
crys = crystalline polymer property
d = dispersed phase
g = gas property
i = penetrant i
j = penetrant j
k = active site type
p = polymer property

Appendix A: Numerical Solution of the RPPFM

To avoid having to solve the moving boundary value problem resulting from the RPPFM (see model eqs 17 and 20), a new dimensionless radial variable, $x(t) = r/R_s(t)$, is introduced. The new variable allows the transformation of the time-dependent radial integration domain into the time-invariant domain $x \in [0, 1]$. Accordingly, the following dimensionless variables are defined

$$Y_{Mi} = C_i/C_{is}$$
$$Y_C^k = C^k/[M_e]_0 A_{sf}^k \qquad \text{(A1)}$$
$$Y_T = T/T_b$$

where Y_{Mi}, Y_C^k, and Y_T are the dimensionless concentrations of monomer i and potential active sites of type k and the dimensionless temperature, respectively. To transform the original system of model eqs 15−25 from the (r, t) independent variables to the (x, t) ones, the partial derivatives of the new dimensionless variables with respect to x and t must be calculated. One can easily show that the partial derivatives ($\partial Y/\partial r$) and ($\partial Y/\partial t$) are given by the following equations

$$\left(\frac{\partial Y}{\partial r}\right) = \left(\frac{\partial Y}{\partial x}\frac{\partial x}{\partial r}\right) = \left(\frac{1}{R_s}\frac{\partial Y}{\partial x}\right) \qquad \text{(A2)}$$

$$\left(\frac{\partial Y}{\partial t}\right) = \left(\frac{\partial Y}{\partial t}\right) + \left(\frac{\partial Y}{\partial x}\frac{\partial x}{\partial t}\right) = \frac{\partial Y}{\partial t} - \frac{r\dot{R}_s}{R_s^2}\frac{\partial Y}{\partial x} \qquad \text{(A3)}$$

where $\dot{R}_s$ is the rate of change of the particle radius, $R_s(t)$. Using the above definitions, the original moving boundary value problem (eqs 15−25) can be recast into the following fixed boundary value problem

Mass balances

$$\frac{\partial Y_{Mi}}{\partial t} = \frac{D_{i,eff}}{R_s^2}\left[\left(\frac{2}{x} + \frac{xR_s\dot{R}_s}{D_{i,eff}} + \frac{1}{D_{i,eff}}\frac{\partial D_{i,eff}}{\partial x}\right)\frac{\partial Y_{Mi}}{\partial x} + \frac{\partial^2 Y_{Mi}}{\partial x^2}\right] + \frac{R_{Mi}}{C_{is}} \qquad \text{(A4)}$$

Initial condition

$$Y_{Mi} = 1 \qquad \text{at } t = 0 \qquad \text{(A5)}$$

Boundary conditions

$$\partial Y_{Mi}/\partial x = 0 \qquad \text{at } x = 0$$
$$Y_{Mi} = (1 - e^{-k_s t}) \qquad \text{at } x = 1 \qquad \text{(A6)}$$

Initial condition

$$Y_T = 1 \qquad \text{at } t = 0 \qquad \text{(A8)}$$

Energy balance

$$\frac{\partial Y_T}{\partial t} = \frac{k_e}{R_s^2 \rho_\rho C_p}\left[\left(\frac{2}{x} + \frac{\rho_\rho C_p \dot{R}_s R_s x}{k_e}\right)\frac{\partial Y_T}{\partial x} + \frac{\partial^2 Y_T}{\partial x^2}\right] + \frac{1}{T_b \rho_p C_p}\sum_{i=1}^{n} MW_i[(-\Delta H_{r,i})R_{Mi}] \quad \text{(A7)}$$

Boundary conditions

$$\partial Y_T/\partial x = 0 \qquad \text{at } x = 0$$

$$\partial Y_T/\partial x = R_s h(1 - Y_T)/k_e \qquad \text{at } x = 1 \quad \text{(A9)}$$

Mass species balances

$$\frac{\partial Y_C^k}{\partial t} = \frac{R_c^k}{[M_e]_0 A_{sf}^k} + \frac{r\dot{R}_s}{R_s^2}\frac{\partial Y_C^k}{\partial x} \qquad c = S_p, P_0, \lambda_0 \quad \text{(A10)}$$

Initial condition

$$Y_C^k = 1 \qquad \text{at } t = 0 \quad \text{(A11)}$$

Boundary condition

$$\partial Y_C^k/\partial x = 0 \qquad \text{at } x = 0 \quad \text{(A12)}$$

The transformed RPPFM consists of a system of stiff nonlinear partial differential equations (eqs A4−A12), as well as a number of algebraic equations for the calculation of the relevant species rate functions (see eqs 1−6), the thermodynamic equilibrium monomer concentration in the particle, and the the internal and external mass- and heat-transfer coefficients.

The above system of partial differential equations was solved by the global collocation method[39] to predict the time evolution of the monomer concentration and temperature profiles in a catalyst/polymer particle.

Literature Cited

(1) Hoel, E. L.; Cozewith, C.; Byrne, G. D. Effect of Diffusion on Heterogeneous Ethylene Propylene Copolymerization. *AIChE J*. **1994**, *40*, 1669.

(2) Hutchinson, R. A.; Chen, C. M.; Ray, W. H. Polymerization of Olefins through Heterogeneous Catalysis X: Modeling of Particle Growth and Morphology. *J. Appl. Polym. Sci*. **1992**, *44*, 1389.

(3) Ferrero, M. A.; Chiovetta, M. G. Effects of Catalyst Fragmentation during Propylene Polymerization. IV: Comparison between Gas-Phase and Bulk Polymerization Processes. *Polym. Eng. Sci*. **1991**, *31*, 904.

(4) Soares, J. B. P.; Hamielec, A. E. General Dynamic Mathematical Modelling of Heterogeneous Ziegler−Natta and Metallocene Catalyzed Copolymerization with Multiple Site Types and Mass and Heat Transfer Resistances. *Polym. React. Eng*. **1995**, *3*, 261.

(5) Sun, J.; Eberstein, C.; Reichert, K. H. Particle Growth Modeling of Gas-Phase Polymerization of Butadiene. *J. Appl. Polym. Sci*. **1997**, *64* (2), 203.

(6) Debling, J. A.; Ray, W. H. Heat and Mass Transfer Effects in Multistage Polymerization Processes: Impact Polypropylene. *Ind. Eng. Chem. Res*. **1995**, *34*, 3466.

(7) Galvan, R.; Tirrell, M. Molecular Weight Distribution Predictions for Heterogeneous Ziegler−Natta Polymerization Using a Two-Site Model. *Chem. Eng. Sci*. **1986**, *41*, 2385.

(8) McKenna, T. F.; Dupuy, J.; Spitz, R. Modelling of Transfer Phenomena on Heterogeneous Ziegler−Natta Catalysts: Differences between Theory and Experiment in Olefin Polymerization (An Introduction). *J. Appl. Polym. Sci*. **1995**, *57*, 371.

(9) Parasu Veera, U.; Weickert, G.; Agarwal, U. S. Modeling Monomer Transport by Convection during Olefin Polymerization. *AIChE J*. **2002**, *48*, 1062.

(10) Kosek, J.; Grof, Z.; Novak, A.; Stepanek, F.; Marec, M. Dynamics of Particle Growth in Gas-Phase Polymerization Reactors. *Chem. Eng. Sci*. **2001**, *56*, 3951.

(11) Sanchez, I. C.; Lacombe, R. H. Statistical Thermodynamics of Polymer Solutions. *Macromolecules* **1978**, *11*, 1145.

(12) Orbey, H.; Bokis, C. P.; Chen, C.-C. Equation of State Modeling of Phase Equilibrium in the Low-Density Polyethylene Process: The Sanchez−Lancombe, Statistical Associating Fluid Theory and Polymer−Soave−Redlich−Kwong Equations of State. *Ind. Eng. Chem. Res*. **1998**, *37*, 4481.

(13) Nicollela, C.; Van Loosdrecht, M. C. M.; Heijnen, J. J. Mass Transfer and Reaction in a Biofilm Airlift Suspension Reactor. *Chem. Eng. Sci*. **1998**, *53*, 3951.

(14) Wacao, N.; Smith, J. M. Diffusion and Reaction in Porous Catalysts. *Chem. Eng. Sci*. **1964**, *3*, 321.

(15) Hatzantonis, H.; Yiannoulakis, H.; Yiagopoulos, A.; Kiparissides, C. Recent Developments in Modeling Gas-Phase Catalyzed Olefin Polymerization Fluidized Bed Reactors: The Effect of Bubble Size Variation on the Reactor's Performance. *Chem. Eng. Sci*. **2000**, *55*, 3237.

(16) Aris, R. *The Mathematical Theory of Diffusion and Reaction in Permeable Catalysts*; Clarendon Press: Oxford, U.K., 1975.

(17) Capek, P.; Hejtmanek, V.; Solcova, O.; Klusacek, K.; Schneider, P. Gas Transport in Porous Media Under Dynamic Conditions. *Catal. Today* **1997**, *38*, 31.

(18) Cussler, E. L. *Diffusion Mass Transfer in Fluid Systems*; Cambridge University Press: Cambridge, U.K., 1997.

(19) Yiagopoulos, A.; Yiannoulakis, H.; Kiparissides, C. Heat and Mass Transfer Phenomena during the Early Growth of a Catalyst Particle in Gas-Phase Olefin Polymerization: The Effect of Prepolymerization Temperature and Time. *Chem. Eng. Sci*. **2001**, *56*, 3979.

(20) Chen, C. M. Gas Phase Olefin Copolymerization with Ziegler−Natta Catalysts. Ph.D. Thesis, University of Wisconsin-Madison, Madison, Wisconsin, 1991.

(21) McHugh, M.; Krukonis, V. *Supercritical Fluid Extraction*, 2nd ed.; Butterworth-Heinemann Publishing: Woburn, MA, 1994.

(22) Michaels, A. S.; Bixler, H. J. Solubility of Gases in Polyethylene. *J. Polym. Sci*. **1961**, *50*, 393.

(23) Kreituss, A.; Freich, H. L. Free Volume Estimates in Heterogeneous Polymer Systems. I. Diffusion in Crystalline Ethylene−Propylene Copolymers. *J. Polym. Sci. B: Polym. Phys*. **1981**, *19*, 889.

(24) Floyd, S.; Choi, K. Y.; Taylor, T. W.; Ray, W. H. Polymerization of Olefins Through Heterogeneous Catalysis—IV. Modeling of Heat and Mass Transfer Resistance in the Polymer Particle Boundary Layer. *J. Appl. Polym. Sci*. **1986**, *31*, 2231.

(25) Kiparissides, C.; Dimos, V.; Boultouka, T.; Anastasiades, A.; Chasiotis, A. An Experimental and Theoretical Investigation of Solubility and Diffusion of Ethylene in Semi-crystalline PE at Elevated Pressures and Temperatures. *J. Appl. Polym. Sci*. **2003**, *87*, 953.

(26) Han-Adebekun, G. C. Heterogeneous Catalyzed Gas Phase Polymerization of Olefins: Kinetic Studies and Modeling Investigations. Ph.D. Thesis, University of Wisconsin-Madison, Madison, Wisconsin, 1996.

(27) Desilets, M.; Proulx, P.; Soucy G. Modelling of Multicomponent Diffusion in High-Temperature Flows. *Int. J. Heat Mass Transfer* **1997**, *40*, 4273.

(28) Benes, N.; Verweij, H. Comparison of Micro- and Microscopic Theories Describing Multicomponent Mass Transport in Microporous Media. *Langmuir* **1999**, *15*, 8292.

(29) Doong, S. J.; Ho, W. S. W. Diffusion of Hydrocarbons in Polyethylene. *Ind. Eng. Chem. Res*. **1992**, *31*, 1050.

(30) Froment, F. G.; Bishoff, K. B. *Chemical Reactor Analysis and Design*; John Wiley & Sons: New York, 1979.

(31) Tucker, C. L. *Fundamentals of Computer Modeling for Polymer Processing*; Hansen Publishers: Munich, 1989.

(32) Van Krevelen, D. W. *Properties of Polymers*; Elsevier Science B.V.: Amsterdam, The Netherlands, 1997.

(33) Kunii, D.; Levenspiel, O. *Fluidization Engineering*, 2nd ed.; Butterworth-Heinemann Publishing: Woburn, MA, 1991.

(34) Ranz, W. E.; Marshall, W. R. Evaporation from Drops. *Chem. Eng. Prog*. **1952**, *48*, 141.

(35) Calderbank, P. H.; Moo-Young, M. B. The Continuous Phase Heat and Mass Transfer Properties of Dispersions. *Chem. Eng. Sci.* **1961**, *16*, 39.

(36) Hetsroni, G. Particles−Turbulence Interaction. *Int. J. Multiphase Flow* **1989**, *15*, 735.

(37) Crowe, C. T. On Models for Turbulence Modulation in Fluid-Particle Flows. *Int. J. Multiphase Flow* **2000**, *26*, 719.

(38) Kanellopoulos, V.; Dompazis, G.; Tsiliopoulou, E.; Kiparissides, C. An Experimental and Theoretical Investigation on the Diffusion of Olefins in Semi-Crystalline Polymers: The Influence of Swelling in Polymer−Penetrant Systems. Presented at the 8th International Workshop on Polymer Reaction Engineering (DECHEMA), Hamburg, Germany, Oct 3−6, 2004.

(39) Villadsen, J.; Michelsen, M. L. *Solution of Diffential Equation Models by Polynomial Approximation*; Prentice-Hall: Upper Saddle River, NJ, 1978.

Received for review November 3, 2003
Revised manuscript received March 17, 2004
Accepted May 12, 2004

IE030810U